JOURNAL OF GEOPHYSICAL RESEARCH, VOL. 105, NO. C7, PAGES 16,923–16,939, JULY 15, 2000

Indian Ocean Warming of 1997–1998

Lisan Yu
Department of Physical Oceanography, Woods Hole Oceanographic Institution, Woods Hole, Massachusetts

Michele M. Rienecker
Oceans and Ice Branch, Laboratory of Hydrospheric Processes, NASA Goddard Space Flight Center, Greenbelt, Maryland

Abstract. The Indian Ocean underwent substantial changes in 1997–1998. The observations show not only the appearance of a dipole mode in the tropical region but also a persistent basin-scale warming. We present in this study an analysis of the basin-scale sea surface temperature (SST) variations during 1997–1998 using satellite observations, in situ temperature measurements, and National Centers for Environmental Prediction reanalyses. We find that the Indian SST anomaly peaks occurred at two periods, i.e., November–December–January coinciding with the Niño3 peak and the following April–May–June, and were phase locked to the Indian Ocean seasonal cycle. The changes of SST in the equatorial ocean were related to a coupled interaction between the atmosphere and the ocean. Oceanic upwelling in the east and downwelling in the west played a major role in giving rise to the SST anomalies associated with the dipole mode structure. The upwelling off the coast of Sumatra elevated the regional thermocline by more than 80 m in December 1997. On the other hand, the changes of SST in the southern Indian Ocean were largely induced by the changes of local latent flux. During boreal fall–winter of 1997 the southeasterly trades were displaced and abnormally prolonged in their northernmost equatorial position. This shifted the center of the trades toward the equator, weakened the winds in the central Southern Ocean, reduced the latent heat flux in the region, and subsequently induced a surface warming. The total change of the SST anomalies integrated over the two periods, July–December 1997 and January–May 1998, were explained well by the same period latent flux integral in both intensity and pattern. The cross-basin upper ocean temperature sections show that the extratropical warming was rather uniformly distributed in the upper 60 m, further supporting the role of mixed-layer processes in the warming.

1. Introduction

In 1997–1998, while one of the strongest El Niños on record took place in the tropical Pacific [*Yu and Rienecker*, 1998; *McPhaden*, 1999], a record-breaking sea surface warming occurred in the entire Indian Ocean and persisted for several seasons [*Yu and Rienecker*, 1999). Meanwhile, an eventful sea surface cooling occurred off the coast of Sumatra in contrast to the warming condition elsewhere in the Indian Ocean. The cooling in the east and warming in the west were strong enough to reverse the climatological sea surface temperature (SST) gradient along the equator [*Webster et al.*, 1999; *Yu and Rienecker*, 1999] and to induce considerable wind and precipitation anomalies [*Anderson*, 1999]. These unusual developments led to the recognition of an existence of a major mode, the so-called dipole mode, in the Indian Ocean [*Webster et al.*, 1999; *Saji et al.*, 1999; *Anderson*, 1999].

The simultaneous ocurrence of the tropical Indian Ocean dipole mode (negative SST anomalies in the east and positive SST anomalies in the west) and the El Niño-Southern Oscillation (ENSO) in 1997–1998 seems to suggest a possible link between these two phenomena. However, by analyzing the historical record both *Webster et al.* [1999] (hereinafter referred to as WMLL99) and *Saji et al.* [1999] (hereinafter referred to as SGVY99) pointed out otherwise: the Indian Ocean dipole mode is independent of ENSO at least to the first degree. This finding is consistent with the earlier observational and theoretical studies. For example, *Reverdin et al.* [1986] and *Kapala et al.* [1994] noted that the Indian Ocean warming in 1962 occurred in the absence of El Niño though it had an El Niño-like structure. *Nicholls* [1978, 1995] discussed monsoon variability and its relation to non-ENSO-related variability within the Indian Ocean. Nevertheless, the ENSO influ-

Paper number 2000JC900068.
0148-0227/00/2000JC900068$09.00

ence is nonnegligible as the Indian Ocean warming (as well as the dipole mode) occurred during several previous ENSO events, particularly during the major events of 1972, 1982, and 1987 [e.g., *Cadet*, 1985; *Yasunari*, 1987a, b; *Nigam and Shen*, 1993; *Tourre and White*, 1995; *Nicholson*, 1997; *Chambers et al.*, 1999]. In other words the ENSO forcing might create a favorable condition, which promotes the manifestation of the Indian Ocean variability.

El Niño can influence the Indian Ocean through the atmospheric connection, namely, the Southern Oscillation (SO) [*Bjerknes*, 1969; *Rasmusson and Wallace*, 1982]. The SO represents large-scale sea level pressure fluctuations between the southeast Pacific and north Australia/Indonesia and defines the associated atmospheric zonal circulations (namely, the Walker Circulations) in both the equatorial Pacific and Indian Oceans [e.g., *Webster*, 1987; *Philander*, 1990]. However, the atmospheric circulation in the Indian Ocean is rather complicated by itself because of the presence of the annually reversing monsoon. This highly variable background mingles with the imposed ENSO signal and complicates the circumstances under which the Indian Ocean variability can be manifested. The 1997–1998 Indian Ocean event was atypical: the persistence, intensity, and scale of the multiseason SST anomalies were all historically high. With the unprecedented availability of satellite observations and an expanded in situ observing network including the Volunteer Observing Ships (VOS) program the 1997–1998 warm event in the Indian Ocean has been the best documented one to date. The data provide a unique opportunity for a detailed process study.

In this paper we present a data analysis of the 1997–1998 Indian Ocean warming and focus on examining two issues, i.e., the primary processes that gave rise to multiseasonal SST anomalies in the Indian Ocean and the possible influence of the El Niño forcing on the warming development. By analyzing a single event we limit ourselves to describing the findings from the data rather than making or testing any general hypothesis. The recent studies of WMLL99 and SGVY99 have analyzed a longer data set and provided a greater insight to the Indian Ocean dipole mode. In particular, the coupled atmosphere ocean interaction in the tropical Indian Ocean is postulated as an important oscillation mechanism. This study, aside from focusing on one event, differs from the two studies on the analysis of the basin-scale SST anomalies, a persistent and prominent phenomenon during 1997-1998. *Chambers et al.* [1999] conducted an empirical orthogonal function (EOF) analysis for SST and sea surface height (SSH) anomalies between 1982 and 1997 and suggested that the Indian Ocean ENSO-related warming is driven by wind-forced Rossby waves associated with the SO. The finding is similar to those of *Tourre and White* [1995, 1997], who postulated ENSO as a "global signal" associated with a coupled ocean–atmosphere wave. In our previous report [*Yu and Rienecker*, 1999] (hereinafter referred to as YR99) we showed that the change of SST in the extratropics was primarily a direct response to the change of local surface air-sea fluxes (the latent flux in particular). This result is supported by the ocean modeling study of *Murtugudde et al.* [2000], who examined the SST anomalies in the Indian Ocean spanning 1958–1998. Although the model had difficulty in simulating the observed anomaly in the southern Indian basin (probably related to the lack of the Indonesian Throughflow), the SST variability in other Indian basins was largely reproduced. The present study is a continuation of YR99. We include the analysis of the upper ocean temperature structures along two cross-basin VOS lines to delineate further the role of the mixed layer dynamics in the extratropical warming.

Multisensor satellite observations, in situ temperature profiles from VOS provided by the Global Temperature–Salinity Profile Program (GTSPP), and model outputs from National Centers for Environmental Prediction (NCEP) reanalyses [e.g., *Kalnay et al.*, 1996] are used. The data and their brief description are given in section 2. The characteristics of nonseasonal variations in 1997–1998 are described in section 3, and the relationship of the SST anomalies with the basin-scale dynamics and ENSO forcing is examined in section 4. The change of surface fluxes and its role in the change of SST is analyzed in section 5. Upper ocean temperature structures along two VOS routes are examined in section 6. Summary and discussions are included in section 7.

2. Data

The following is the list of data sets used in the study. A brief description of each data set is included.

1. SSTs are from the Reynolds analyses [*Reynolds and Smith*, 1995]. The data are obtained by optimally interpolating satellite SSTs from the advanced very high resolution radiometer (AVHRR) with in situ SST measurements. Monthly and weekly means on the 1° grid are used. Unless specified, the SST anomalies in the study are calculated as the departures from the 1982–1996 base period monthly means.

2. SSHs are from the TOPEX/Poseidon altimeter. The processing procedure, which is described by *Adamec* [1998], includes all standard corrections. Cycle means (1 cycle $\approx$ 9.98 days) with 1°$\times$ 1° resolutions are used. The cycle anomalies are computed using the 1993–1996 base period monthly means.

3. Surface wind products of Special Sensor Microwave Imager (SSMI) [*Atlas et al.*, 1993]. These data are derived from a blend of wind speed observations from the Defense Mapping Satellite Program SSMI, wind vectors from ship and buoy observations, and surface wind analyses from the European Centre for Medium Range

Weather Forecasts (ECMWF). The data are 6 hourly with a resolution of 2.5° in longitude and 2° in latitude. Monthly means are computed, and the anomalies are derived from the 1988–1996 base period monthly means.

4. Surface heat fluxes diagnosed from the NCEP reanalyses [*Kalnay et al.*, 1996]. The daily model outputs are used to calculate monthly climatologies for each of the flux components (latent, sensible, net shortwave, and net longwave). The 15 year period 1982–1996 is the base on which anomalies are computed.

5. Upper ocean temperature profiles from the database of the GTSPP. In situ temperature measurements in the Indian Ocean are available along a few VOS routes. For the purpose of our basin-scale analysis we utilize the temperature profiles along two cross-basin VOS lines: one is between Madagascar and Sumatra, and the other is between Somalia and Shark Bay in Australia. Because ships along these two VOS lines were operated rather infrequently and irregularly, it is not possible to derive a complete time series of upper ocean structure on a monthly basis or even the long-term mean state. To delineate the changes occurring in 1997–1998, we compare with the upper ocean structure of 1995–1996.

The first three data types (SST, SSH, and wind) are identical to those used by WMLL99, although some data sets might come from different sources. For instance, the SSMI wind products used by YR99 and this study are from an optimal blending of satellite, in situ, and model data, while the NCEP winds used by WMLL99 are the data-assimilated model products. Nevertheless, the two wind products are qualitatively consistent during the whole targeted period (not shown). It should also be noted that this study includes the NCEP diagnosed heat fluxes and VOS subsurface temperature measurements as additional data sets, while WMLL99 analyzed the outgoing longwave radiation. WMLL99 focused on the internal ocean dynamics and on the internal (to the Indian Ocean) coupled ocean-atmosphere dynamics during this event. This paper focuses on the role of the surface heat flux forcing in the basin-wide warming and on the variations of the SST anomalies around the Indian Ocean.

3. Evolution of the Surface Fields in 1997–1998

3.1. Mean Fields

The atmospheric circulation in the Indian Ocean is strongly influenced by the annually reversing Indian Monsoon and has a distinct seasonal cycle [*Webster*, 1987; *Shukla*, 1987]. This is seen in Figure 1a, the monthly averaged climatological surface wind fields in August, November, February, and May. While southwesterlies prevail in the boreal summer, northeasterlies prevail in the boreal winter. The southeast (SE) trades dominate the southern tropical Indian Ocean throughout the year, strongest and closest to the equator during the summer and vice versa during the winter. The central and eastern equatorial regions are generally a weak wind zone. Equatorial westerlies are observed during

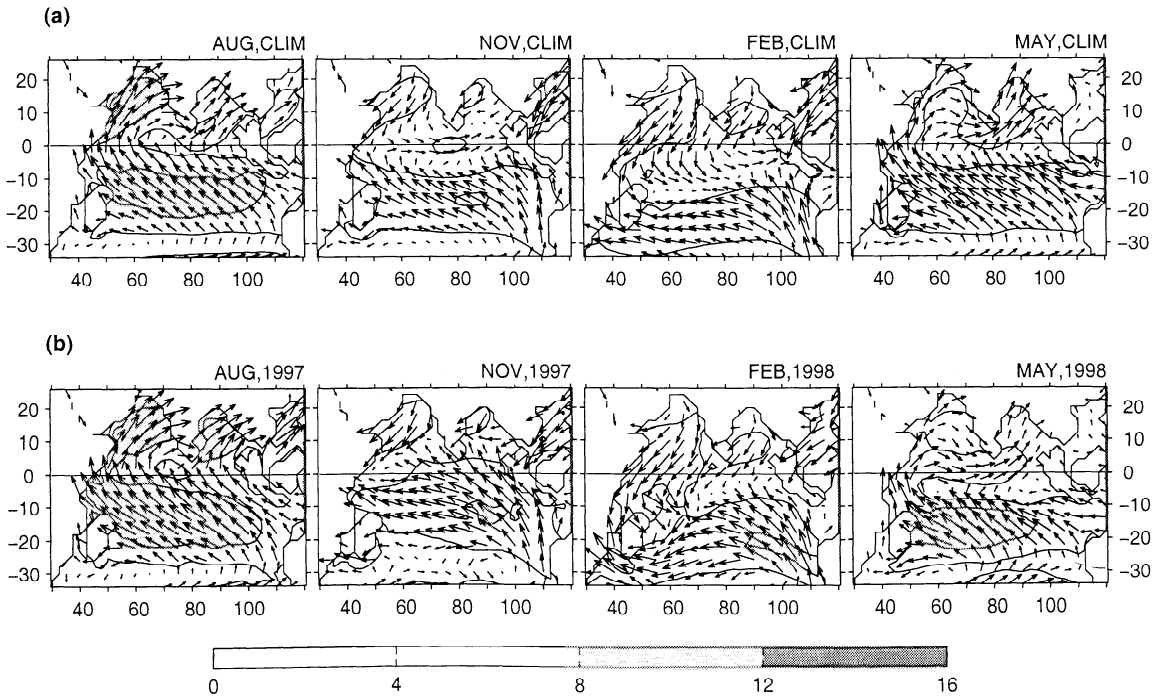

Figure 1. The monthly mean SSMI wind fields in August, November, February, and May during (a) a climatological year and (b) 1997–1998. Wind speeds greater than 8 m s^{-1} are shaded. The contour interval is 4 m s^{-1}.

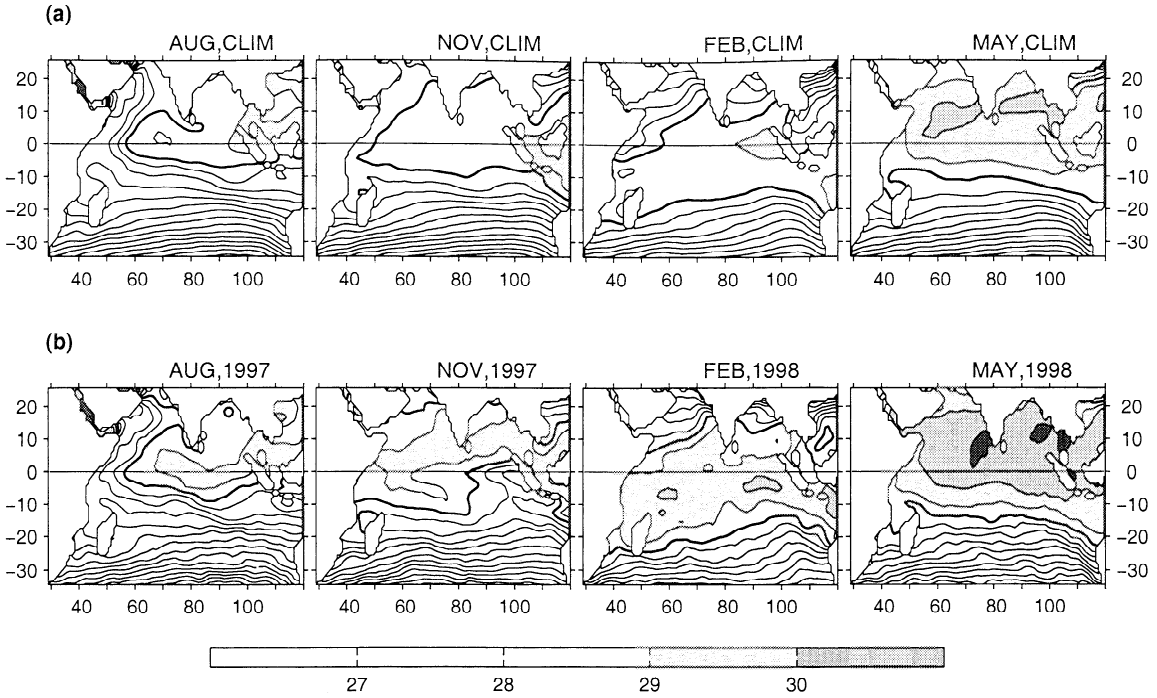

Figure 2. The monthly mean Reynolds SST fields in August, November, February, and May during (a) a climatological year and (b) 1997–1998. The 28°C isotherm is thickened, and SSTs higher than 29°C are shaded. The contour interval is 1°C.

monsoon transitions, most evident in the fall, revealing the influence of the Walker Circulation in the Indian Ocean.

The seasonal evolution of the climatological SST is displayed in Figure 2a for the same 4 months. SST and surface winds are closely correlated, with the surface winds in both hemispheres crossing isotherms toward the warmest water. The isotherms in the Southern Ocean migrate latitudinally in accord with the annual march of solar heating, closer to the equator in July–August and farther away in January–February. This brings seasonal variations in the strength of the meridional gradient of SST and, accordingly, the intensity and position of the SE trades.

The monthly mean surface wind and SST fields in 1997–1998 are shown in Figures 1b and 2b, respectively. The changes occurring during August 1997 and May 1998 are the focus of this study. Compared with the corresponding climatological state, the SE trades were stronger and the sea surface was warmer north of the equator during the summer of 1997. The changes became significant in the fall of 1997. At that time the equatorial region observed unusual easterly winds in contrast to the climatological westerlies. The SE trades were displaced abnormally equatorward and did not proceed on their seasonal retreat. Meanwhile, the zonal SST gradient along the equator was reversed. With a pool of warmer water in the west and a tongue of cooler water in the east off the coast of Sumatra the region looked more like the tropical Pacific Ocean in non-El Niño years. These alterations in the equatorial atmosphere-ocean were the manifestation of the reversal of the Indian Walker Circulation [*Webster*, 1987]. During the winter of 1998, while the surface wind was reverting gradually to its climatological state, the recovery of the normal SST pattern in the east proceeded quickly. The rapid rise in SST was not limited to the eastern equatorial region but rather occurred over the whole basin. By the spring of 1998 the sea surface had warmed up basin-wide, most evident in the region north of 10°S where exceptionally high SSTs greatly amplified the local seasonal maximum. The broad warming in the Indian Ocean waned after the summer of 1998.

3.2. Nonseasonal Variability

To identify the nonseasonal variability, the anomalous surface wind and SST fields are given in Figures 3–4 at 2 month intervals from July 1997 to May 1998. Anomalous equatorial easterly winds began to develop in early summer of 1997. This development accompanied the prolonged equatorward displacement of the SE trades, resulting in the weakened winds across the southern basin. Meanwhile, anomalous cold surface water appeared off the coast of Sumatra because of the strengthened upwelling (WMLL99) and extended westward and equatorward. By November 1997 the negative SST anomalies in the eastern basin were more than 3°C, and the positive anomalies in the western equatorial region were above 1°C. These anomalies were of

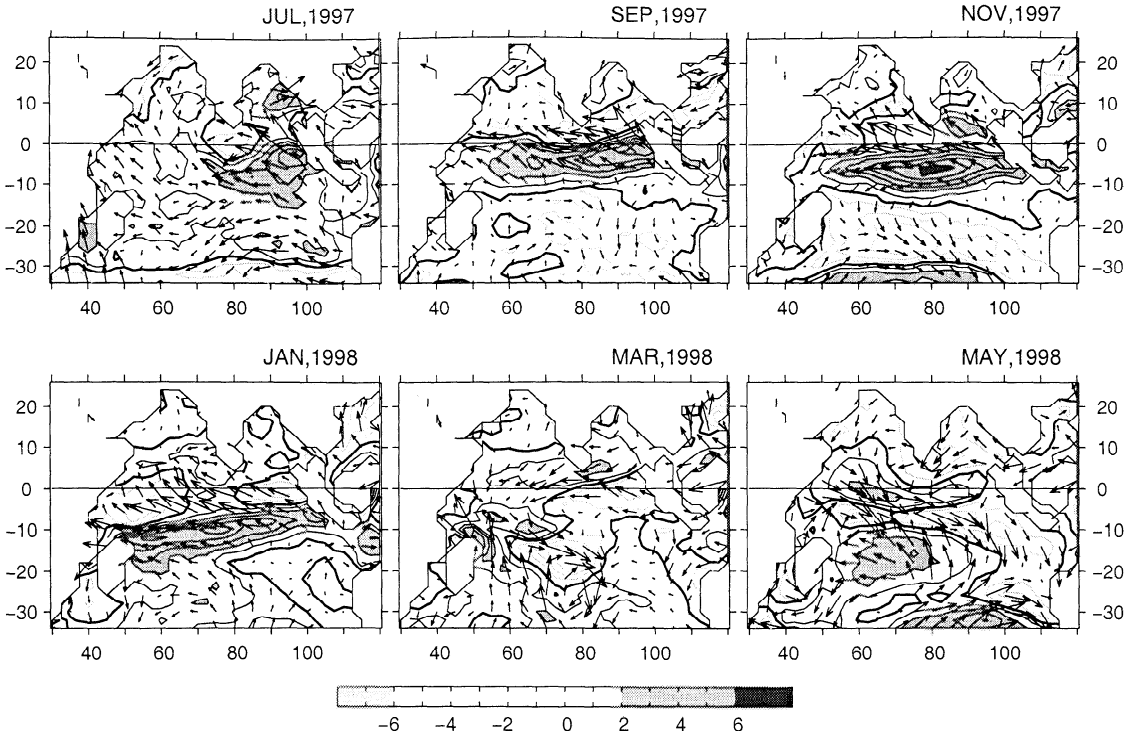

Figure 3. The monthly mean anomalous SSMI wind fields during July 1997 through May 1998 at 2 month intervals. Zero lines are thickened. Speed anomalies are in darkly shaded if >2 m s^{-1} and lightly shaded if < -2 m s^{-1}. The contour interval is 1 m s^{-1}.

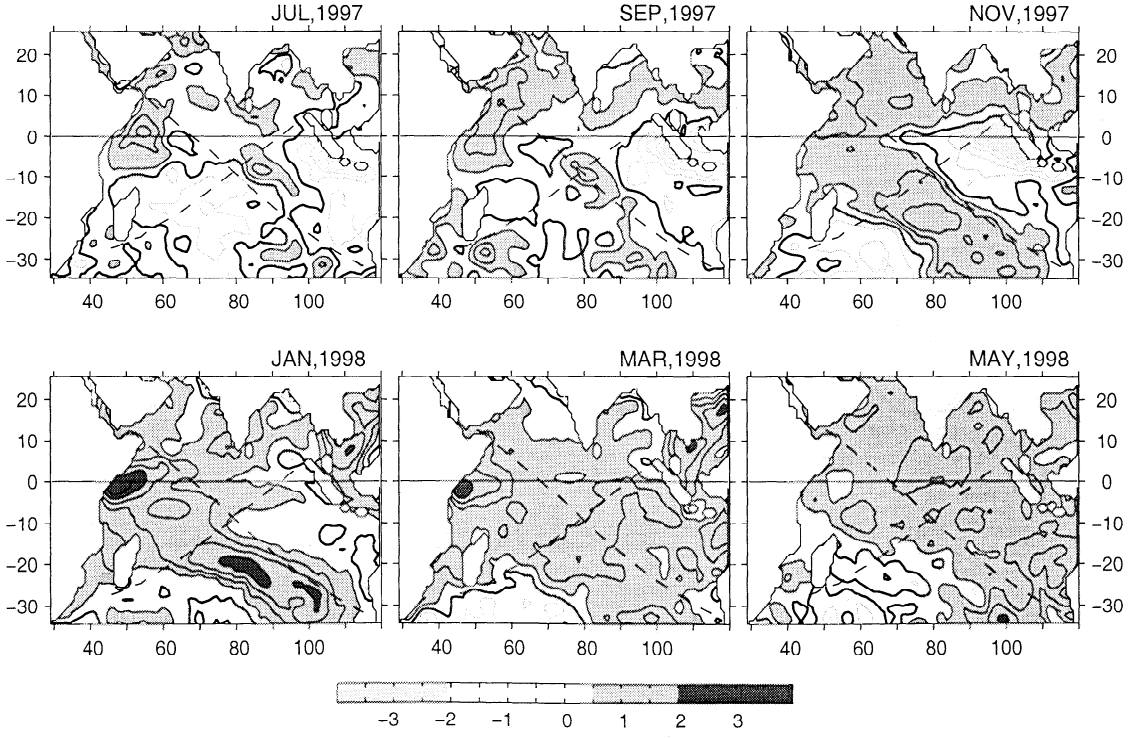

Figure 4. The monthly mean anomalous SST fields during July 1997 through May 1998 at 2 month intervals. Zero lines are thickened. SST anomalies are darkly shaded if > 0.5°C and lightly shaded if < -0.5°C. The contour interval is 0.5°C. The two cross-basin dashed lines are the VOS routes.

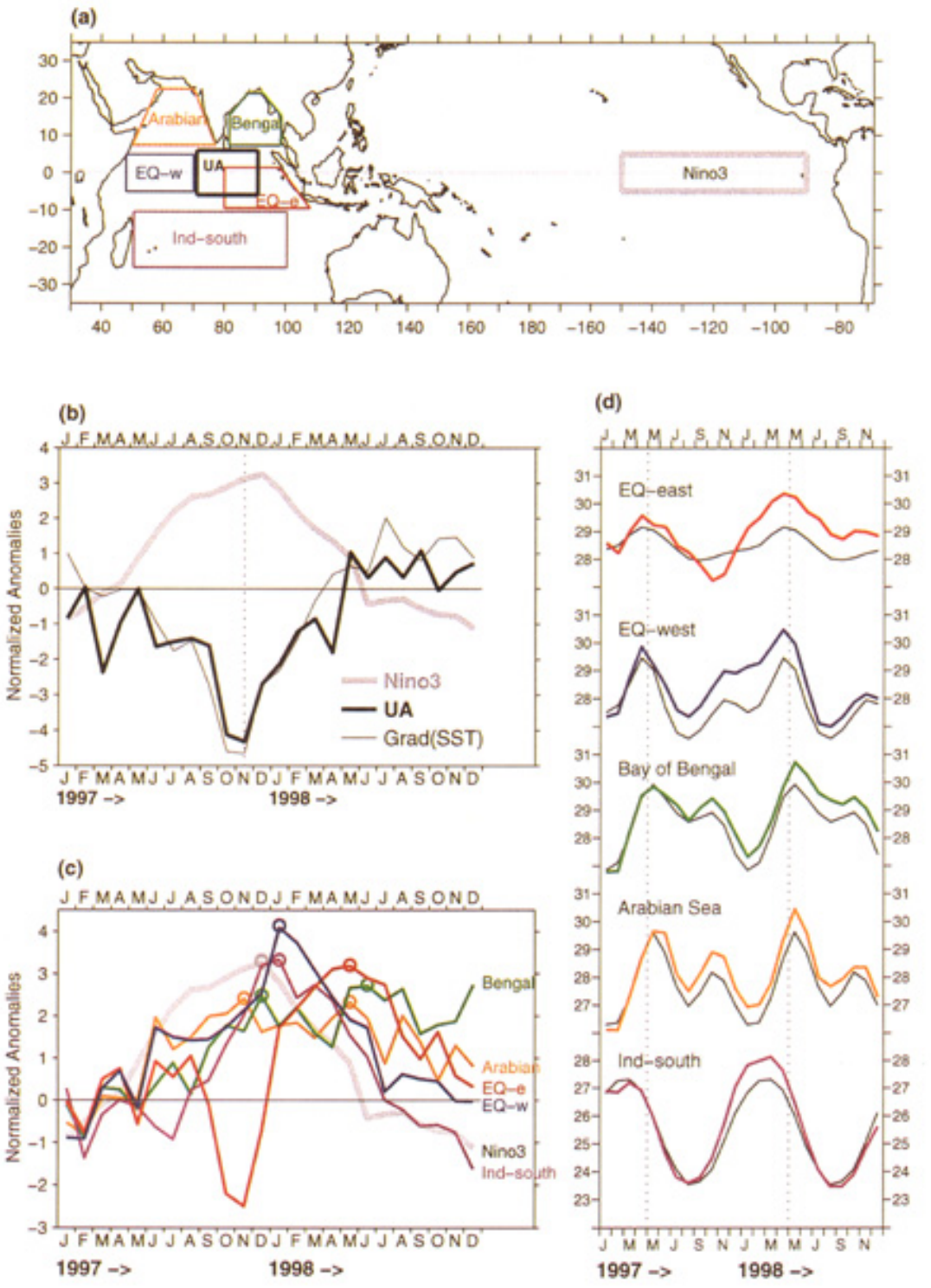

Plate 1. (a) The locations of the Indian Ocean and the Pacific Ocean Niño3 indices. (b) The Indian dipole indices versus the Niño3 index in 1997–1998. (c) The basin-wide Indian SSTA indices versus the Niño3 index in 1997–1998. Peak values are marked by a circle. (d) Variations of the monthly-mean SST during 1997–1998 (colored lines) with regards to their respective climatological seasonal cycles (shaded lines).

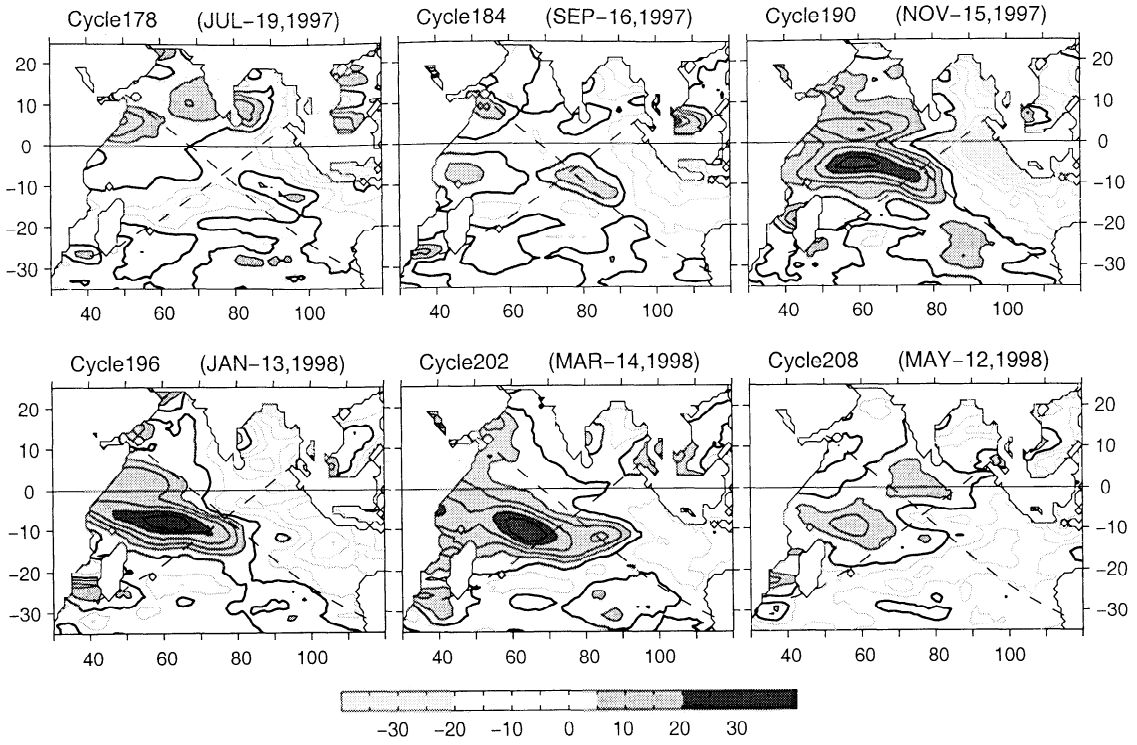

Figure 5. The cycle mean anomalous SSH fields from TOPEX/Poseidon during July 1997 through May 1998 at 2 month intervals. Zero lines are thickened. SSH anomalies are darkly shaded if >5 cm and lightly shaded if < −5 cm. The contour interval is 5 cm. The two cross-basin dashed lines are the VOS routes.

sufficient magnitude to reverse the climatological east-west SST gradient along the equator (Figure 2b). From the beginning of 1998 the sea surface was anomalously warm over the whole Indian Ocean. The magnitude and persistence of the broad-scale warming are shown more explicitly in the SST anomaly plots. Large positive SST anomalies (>1°C) were confined in a banded structure across the southern basin in January 1998. As shown by *Latif et al.* [1999] and *Lau and Wu* [1999], these anomalies forced the anomalous rainfall over East Africa during this period. In March and May 1998 the warming persisted rather uniformly over the whole basin.

As in the Pacific, the changes in the equatorial zonal winds in the Indian Ocean have profound impacts on the regional ocean circulation [e.g., *Cane*, 1980; *McCreary et al.*, 1993; *Yang et al.*, 1998]. This is clearly shown in the anomalous SSH fields derived from the TOPEX/Poseidon altimeter (Figure 5). The studies by YR99, WMLL99, and *Chambers et al.* [1999] provided extensive analyses of SSH data and of the relationship between wind anomalies, SSH signal, and the generation of Kelvin and Rossby waves. Here we present only a brief description of the SSH data and focus on the analysis of the SSH and SST relationship. The easterly anomalies in June–December 1997 generated coastal upwelling off Sumatra as well as equatorial upwelling Kelvin and downwelling Rossby waves (YR99, Figure 1). The upwelling in the eastern basin lifted the thermocline, brought the colder deep water into the surface, and depressed the sea level. Downwelling in the west had the opposite effect on the thermocline. As a result, the sea level tilted toward the west, and the equatorial SSH gradient was reversed. By November 1997 the SSH dropped as much as 30 cm in the eastern equatorial region and rose more than 20 cm in the western basin.

YR99 has reported that during the warming development, negative SST anomalies were directly related to negative SSH anomalies, but the positive SST anomalies were not always associated with positive SSH anomalies. The negative SST (Figure 4) and SSH anomalies in the eastern basin were well correlated because the upwelled colder water directly affected the sea surface temperature. On the other hand, downwelling, which pumps warm surface water into the ocean interior, does not directly increase the SST. The deepened thermocline coincided with the general warming of the sea surface, but the locations of maximum SSH anomalies were not correlated with those of maximum SST anomalies. Major SSH changes were associated with the equatorial Rossby wave structure, centered at ~5° in both hemispheres in late boreal fall 1997. However, major SST variations were confined in a banded structure, aligned away from the equatorial waveguide. The positive SSH signal became more asymmetric about the equator with time; the northern branch shrank and weakened, while

the southern branch extended southeastward with the peak amplitude virtually unchanged. WMLL99 related the southern warming to a ridge of anomalous Ekman convergence just south of the equator during boreal fall–winter 1997. This is consistent with the SSMI wind anomalies during this period (Figure 3). Meanwhile, the positive SST signal spread over the entire Indian basin, and by March 1998 the band of maximum SST anomaly in the Southern Ocean had disappeared. The differences between the rise of the sea surface level and the rise of the SST are more evident between January and June 1998. At that time the SSTs were abnormally high over the entire basin, but the sea levels in the eastern basin remained abnormally low, yielding a negative correlation between the two variables in the eastern basin.

4. Development of the Indian Ocean SST Anomalies

To follow the development of the Indian Ocean SST anomalies (SSTAs) during 1997–1998 and their relation to the evolving El Niño, we divide the Indian Ocean into five regions and use the area-averaged SSTAs as indices. The five regions include two equatorial boxes: EQ-west (5°S–5°N, 50°–70°E) and EQ-east (10°S–2°N, 80°–110°E), and three boxes outside of the equatorial ocean: Arabian (40°–80°E, 7°–22°N), Bay of Bengal (80°–100°E, 7°–22°N), and Ind-south (50°–100°E, 25°–10°S) (Plate 1a). The Niño3 SSTA index is also used, which is the area-averaged SSTA over the Pacific box (5°S–5°N, 150°–90°W). All the SSTA indices are normalized by their own standard deviations.

4.1. Tropical Dipole Mode

Figures 3–5 show that the Indian Ocean mode, presented by WMLL99 and SGVY99, is characterized by negative SST anomalies in the eastern equatorial region, off the coast of Sumatra, and by positive SST anomalies in the western equatorial region. The negative anomalies were associated with enhanced upwelling favorable winds (e.g., WMLL99), while the negative anomalies were associated with anomalous heat fluxes and reduced east–west transports along the equator because of the enhanced easterlies (e.g., SGVY99). These anomalies were coherent with the same sign SSH anomalies and easterly wind anomalies and were the manifestation of the reversal of the Walker Circulation in the Indian Ocean. WMLL99 and SGVY99 described the dipole mode as self-sustaining coupled ocean–atmosphere–land interactions. However, the longtime data record indicates that the ENSO forcing might act as a trigger for the dipole mode development as the dipole mode occurred during previous major El Niño events. SGVY99 and WMLL99 related the decay of the dipole mode to the demise of the El Niño at least during 1997–1998, although, as SGVY99 noted, there are also significant dipole modes during 1961 and 1967, times of no ENSO and a La Niña, respectively. The nature of the ENSO forcing of the Indian dipole mode is beyond the scope of this study.

Here, for completeness we plot the dipole indices of SGVY99 along with the Pacific Niño3 SSTA index (Plate 1b). The index UA denotes the normalized zonal wind anomaly averaged in the area (5°S–5°N, 70°–90°E). The negative value of UV represents easterly wind anomalies. The index Grad(SSTA) is calculated as the difference between the normalized SSTA in the east (EQ-east) and that in the west (EQ-west). The negative value of Grad(SSTA) indicates a reversal of the climatological condition: the surface of the eastern equatorial basin was cooler than that of the western basin. The phasing of the index follows the composite behavior of SGVY99. The easterly wind anomalies and the reversal of Grad(SSTA) developed simultaneously in early summer of 1997. The coupling became strong with time, and the dipole indices reached maximum intensity in October–November 1997, a couple of months earlier than the Niño3 index.

4.2. Basin-Scale SST Anomalies

The comparison between the large-scale SSTA indices and the Niño3 index is plotted in Plate 1c. Three features are clearly shown. First, warming in the equatorial and northern Indian Ocean began to develop in March–April 1997, while the warming in the southern Indian Ocean developed a few months later, in the summer of 1997. Second, evolutions of SSTA in different regions were quite different. The anomaly intensity was maintained for almost a year in the Arabian Sea and Bay of Bengal, unlike those in the EQ-west and Ind-south where they rose quickly during the boreal fall and then fell rapidly after the peak. The eastern equatorial region was the only area where abnormal cooling developed in the middle of the warming episode. Last, the peak timing can be grouped into two periods: November–December–January and the following April–May–June. The first period coincided with the Niño3 peak.

Chambers et al. [1999] conducted an EOF analysis for the Reynolds SST for 1982–1997. The mode 1 map showed that for the Indian Ocean, large warm SST anomalies were located in both the southwestern basin and Arabian Sea and that they were associated with the classic El Niño pattern in the Pacific. Furthermore, the time series indicated that the onset of the warming in these Indian regions was very close to that in the eastern Pacific during major El Niño events of 1983, 1987, and 1997. Our analyses follow the month-to-month development for the 1997–1998 event. To a large degree, the mode 1 structure of *Chambers et al.* [1999] resembles the anomalous SST distribution in November 1997 (Figure 4). At that time, major positive SSTAs ($> 1°C$) were centered in the western Arabian

Sea and central southern Indian Ocean. However, our analyses indicate that the evolutions of SST in these two regions were rather different. The warming in the Arabian Sea started in May 1997, while the warming in the central southern basin occurred later, in August 1997. The warming in the Arabian Sea reached its first peak in November 1997, while the warming in the southern basin was still in development, with its maximum intensity occurring in January 1998. The amplitude of the second peak in the Arabian Sea was similar to that of the first. The changes of SST between these two peaks were less than half of the standard deviation. It appeared that the warming in the Arabian Sea was able to be sustained near its maximum intensity for quite a long period, from October 1997 to June 1998, although the peak moved from off the coast of Somalia to south of India. This feature seems to be not atypical from the comparison with the study of *Nicholson* [1995] in which a harmonic analysis was applied to eight warm ENSO episodes during 1948–1988. The time-space evolution of the composite SSTA in the Arabian Sea [see Nicholson, 1995, Figure 10] showed a similar development: the response of the regional SST to ENSO was at its maximum during September–December of the ENSO year, and the intensity in the northeastern area, after a mild decline, reached the second peak in April–May following the ENSO year. We have also observed two anomaly peaks in the Bay of Bengal, with the first one occurring in December 1997 and the second, stronger, one in June 1998. The regional development before July 1998 was in good agreement with the composite pattern of Nicholson's study, which examined variability up to the month of June in the year following the ENSO peak.

4.3. Correlation With the Seasonal Cycle of the Indian Ocean

Plates 1b–1c reveal that the peak timing of the dipole indices and also the basin-wide SSTA indices have phase shifts with respect to the Niño3 maximum, suggesting a role of the Indian Ocean internal dynamics [WMLL99, *Murtugudde et al.*, 2000]. To see this more clearly, we examine the phase relationship with the seasonal cycle of the Indian Ocean. The evolution of the monthly mean SST in these five regions in 1997–1998 along with their climatological seasonal cycles is plotted in Plate 1d. The influence of the annually reversing Indian Monsoon is clearly shown. Multiple extrema exist in the northern and western regions with high SSTs occurring during monsoon transitions (April–May and October–November) and low SSTs occurring during the monsoon periods (August–September and January–February). The SST seasonal evolution in the eastern equatorial region (EQ-east) is less complicated, with one cycle annually (maximum in April–May and minimum in October–November). The behavior of the southern Indian Ocean (Ind-south) is climatological: the highest SST appears in the local summer (February), and the lowest SST appears in the local winter (August), showing the influence of solar heating on the regional SST.

During 1997–1998 the SSTs in all the regions evolved in accord with their own seasonal cycles, although the amplitudes deviated considerably. Like the ENSO, which is phase-locked to the seasonal cycle in the Pacific [*Rasmusson and Carpenter*, 1982; *Philander*, 1990], the anomaly peaks in the Indian Ocean were also regulated by their own seasonal cycle. The phase locking of the Indian Ocean dipole mode has been noted by SGVY99 and WMLL99. Plates 1c–1d show that except in the EQ-east where the negative SSTA occurred 1–2 months after the seasonal minimum, the SSTA peaks were locked to the seasonal extrema.

5. Role of Heat Fluxes in the Basin-Scale Warming

5.1. Change of the Latent Heat Flux

The SST tendency equation can be expressed as

$$\frac{\partial T}{\partial t} = \frac{Q_{\text{net}}}{\rho c_p H} - \mathbf{u} \cdot \nabla T - w\frac{\partial T}{\partial z} + \text{Diffusion}, \quad (1)$$

where ρ is the water density, c_p is the specific heat, and H is the mixed layer depth. One can see that the change of SST can be attributed to several important processes, such as the net air-sea heat flux, Q_{net} (the sum of latent heat release, solar radiation, longwave radiation, and sensible flux) and horizontal ($\mathbf{u} \cdot \nabla T$) and vertical ($w\partial T/\partial z$) advections. The effect of direct air-sea heat fluxes on SST has been shown to be significant in the extratropical regions of the Indian Ocean and off coasts where ocean wave dynamics are less dominant [*Liu et al.*, 1994; *Gautier et al.*, 1998; *Yang et al.*, 1998]. The impact of these terms is also significant in the warm pool region of the western Pacific and was a major focus of the Tropical Ocean Global Atmospheres/Coupled Ocean Atmosphere Response Experiment (TOGA/COARE) [*Webster and Lukas*, 1992]. YR99 showed that the broad-scale surface warming in the extratropical Indian Ocean during 1997–1998 was largely induced by the change of latent heat flux associated with the change of wind speed. To elucidate this point more clearly, we first show in Figure 6 the monthly SSTA tendency, defined as the differences of the first-week SSTA between 2 consecutive months. Positive SSTA tendency did not occur uniformly in space in contrast to what one might expect from a basin-wide warming (Figure 4). Instead, a warming tendency in one area was often accompanied by a cooling tendency in some other areas. Between September 1997 and April 1998, warming tendency dominated cooling tendency, with the maximum intensity located in the southern basin in the fall of 1997 and then north of 10°S in the first few months of 1998. This continuous warming trend from south to north eventually led to basin-scale positive SSTA in the spring of 1998 (Figure 4).

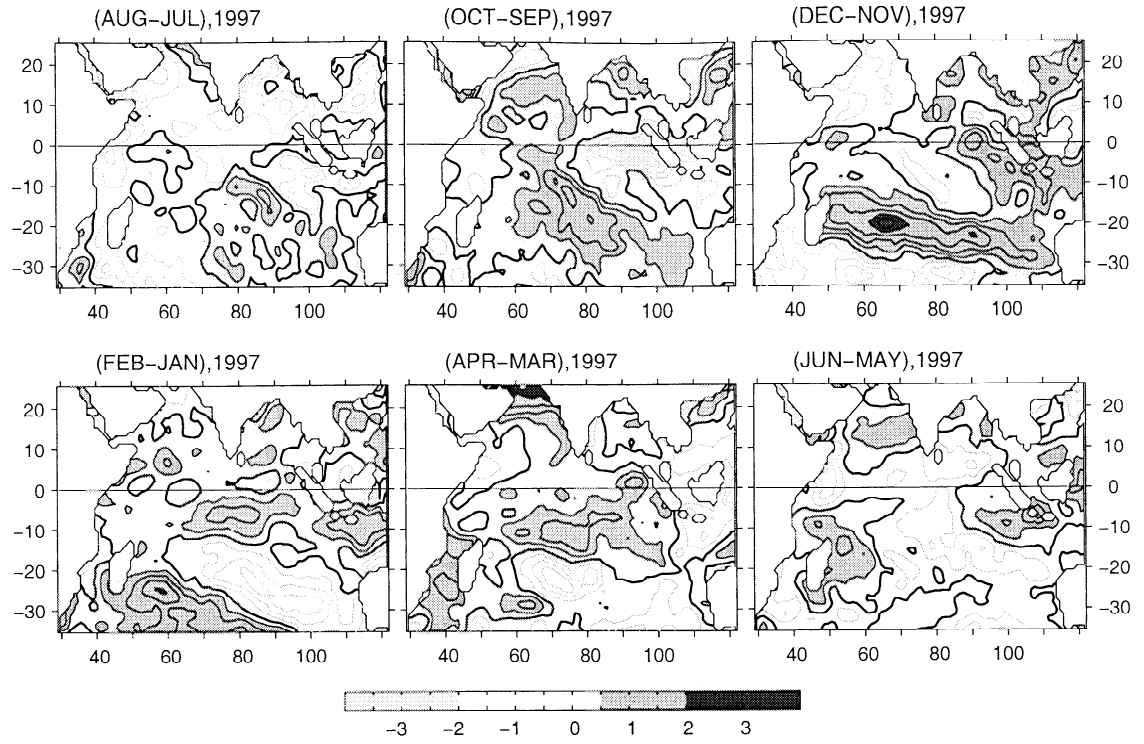

Figure 6. The monthly mean SSTA tendency (defined as the differences of the first-week SST anomalies between 2 consecutive months) during July 1997 through June 1998 at 2 month intervals. The anomalies are darkly shaded if $>0.5°C$ $(month)^{-1}$ and lightly shaded if $< -0.5°C$ $(month)^{-1}$. The contour interval is $0.5°C$ $(month)^{-1}$, and zero lines are thickened.

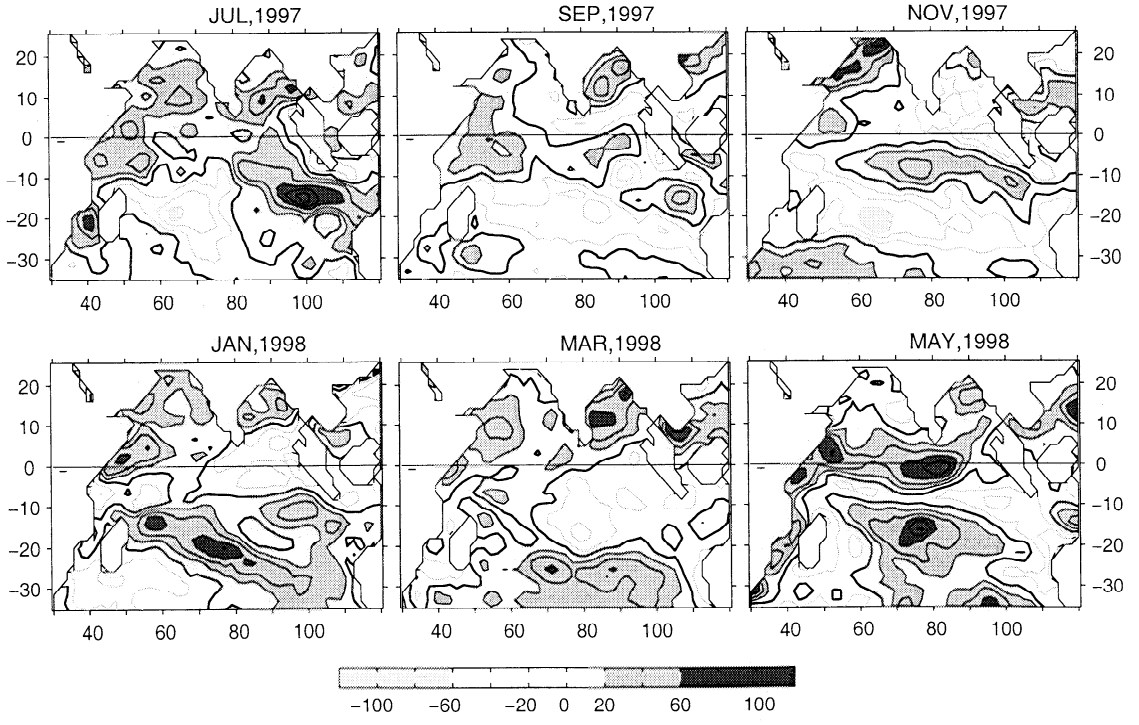

Figure 7. The monthly mean latent heat flux anomalies diagnosed from the NCEP reanalyses for the period July 1997 through May 1998 at 2 month intervals, where the positive (negative) sign denotes more (less) latent heat release from the sea surface. The anomalies are darkly shaded if > 20 W m^{-2} and lightly shaded if < -20 W m^{-2}. The contour interval is 20 W m^{-2}, and zero lines are thickened.

The change of latent heat flux is shown in Figure 7. The surface fluxes are diagnosed from the model output of NCEP reanalyses. The pattern and magnitude of latent flux variations were in good agreement with those of month-to-month SSTA tendency (Figure 6). In particular, the progressive warming in the southern basin between June and December 1997 occurred at the time that the regional latent heat release was persistently reduced. For example, in November 1997, there were negative latent heat flux anomalies across the central Southern Ocean in a banded structure. Its location correlated perfectly with the regional positive SST anomaly center. Moreover, the warming of the eastern tropical region during the first few months of 1998 corresponded directly to the reduced latent heat release in the area. This points out the leading role of the latent flux in the broad-scale Indian Ocean warming.

The diagnosed NCEP heat fluxes are derived from the reanalyses of an atmospheric general circulation model (GCM), which itself is forced by the observed SST. One might wonder whether the latent heat flux anomalies from NCEP were the direct response to the SST anomalies. This is not the case because higher (lower) SST would lead to a greater (weaker) latent heat release if other physical parameters were kept unchanged. What happened here was exactly the opposite: the SST was higher because of less latent heat release. In other words, the changes of latent flux drove the SSTA tendency. YR99 showed that the fluctuations in the latent flux were primarily controlled by the changes of surface wind speed and the NCEP analyses simulated the large-scale perturbations in the surface wind, as measured by the SSMI wind analyses, well. On the broad scale, areas with stronger (weaker) wind speed were mostly consistent with greater (weaker) latent heat release. This is most evident in the southern Indian basin between June and December 1997 and in the eastern equatorial region during the first few months of 1998, indicating the broad-scale warming was due primarily to the changes of latent flux associated with the changes in wind speed.

The large-scale fluctuations in the surface wind speed were related to ENSO at least in the eastern basin. WMLL99 and SGVY99 showed that the atmospheric response to the reversed zonal gradient of SST along the equator is the appearance of easterly anomalies of sufficient strength to reverse the late fall Walker Circulation. The SE trades were displaced longer in their northernmost equatorward position (Figures 1 and 3). These abnormalities strengthened the winds in the equatorial region but weakened the winds over the vast area south of 10°S. The effect was particularly dramatic in the fall of 1997, during which the significantly weakened winds led to a great reduction in the latent heat release. Starting from January 1998, the equatorial easterly anomalies gradually diminished (Figure 3) as El Niño waned. This reduced the upwelling in the eastern Indian Ocean (Figure 5) and reduced the cooling effect on the regional sea surface there, but the sea level was still low. Actually, the quick rise in eastern equatorial SST (Figure 4) in early 1998 can be attributable at least partially to the latent heat flux (the solar heating was another factor as is shown in section 5.2). Two effects operated consecutively for the latent heat reduction in the region. The first effect was that of negative SST anomalies, which had persisted since June 1997 and eventually fed back to latent heat flux through the specific humidity deficit [*Gautier et al.*, 1998]. This is clearly shown in November 1997 when the latent heat flux anomalies responded directly to the regional SST anomalies rather than to regional wind speed anomalies, which were positive at this time. The second effect was that of the weakened wind speed. Between January and May 1998 the abnormal equatorial easterlies were being diminished, but the climatological equatorial westerlies were not resumed. The result was the reduced wind speed and, consequently, the reduced latent heat release in the equatorial region.

5.2. Effects of Other Flux Components

Net surface heat flux consists of four components, the latent heat release, solar heating, longwave radiation, and sensible flux. The above analyses have shown that the latent heat flux was the primary cause of the change of the SST, particularly in the Southern Ocean, during 1997–1998. To examine the overall effect of each flux term on the intensity and timing of the warming, we integrate the tendency and flux terms in (1) over two periods, July–December 1997 and January–May 1998, by setting the mixed layer depth to 60 m (see section 6 for the basin-scale upper ocean structure). Figure 8 plots the total change of SSTA and the change of SSTA induced by latent flux and net radiation (the sum of solar and longwave radiations) over these two periods. The contribution from the sensible flux is small and not shown here. During July–December 1997, major warming was located in the Southern Ocean with the SSTA more than 3°C in the central basin. The heat source appeared to have come from the latent flux, as the pattern and intensity of the SSTA induced by the latent heat agrees well with those of the total SSTA. Similarly, the latent heat flux was also the primary forcing for the cooling of the regional sea surface during January–May 1998.

The net radiation anomalies diagnosed from the NCEP reanalyses were generally <20 W m^{-2} (not shown), about 3 times smaller than the latent flux anomalies. Correspondingly, the contribution of the net radiation to the change of the SST was generally small except in the equatorial region, where the forcing could induce a change of SST up to 1°C (Figure 8). The relatively large contribution of the net radiation in the equatorial region might have resulted from the change of the convection and therefore the cloud pattern in response to the dipole mode and the reversal of the

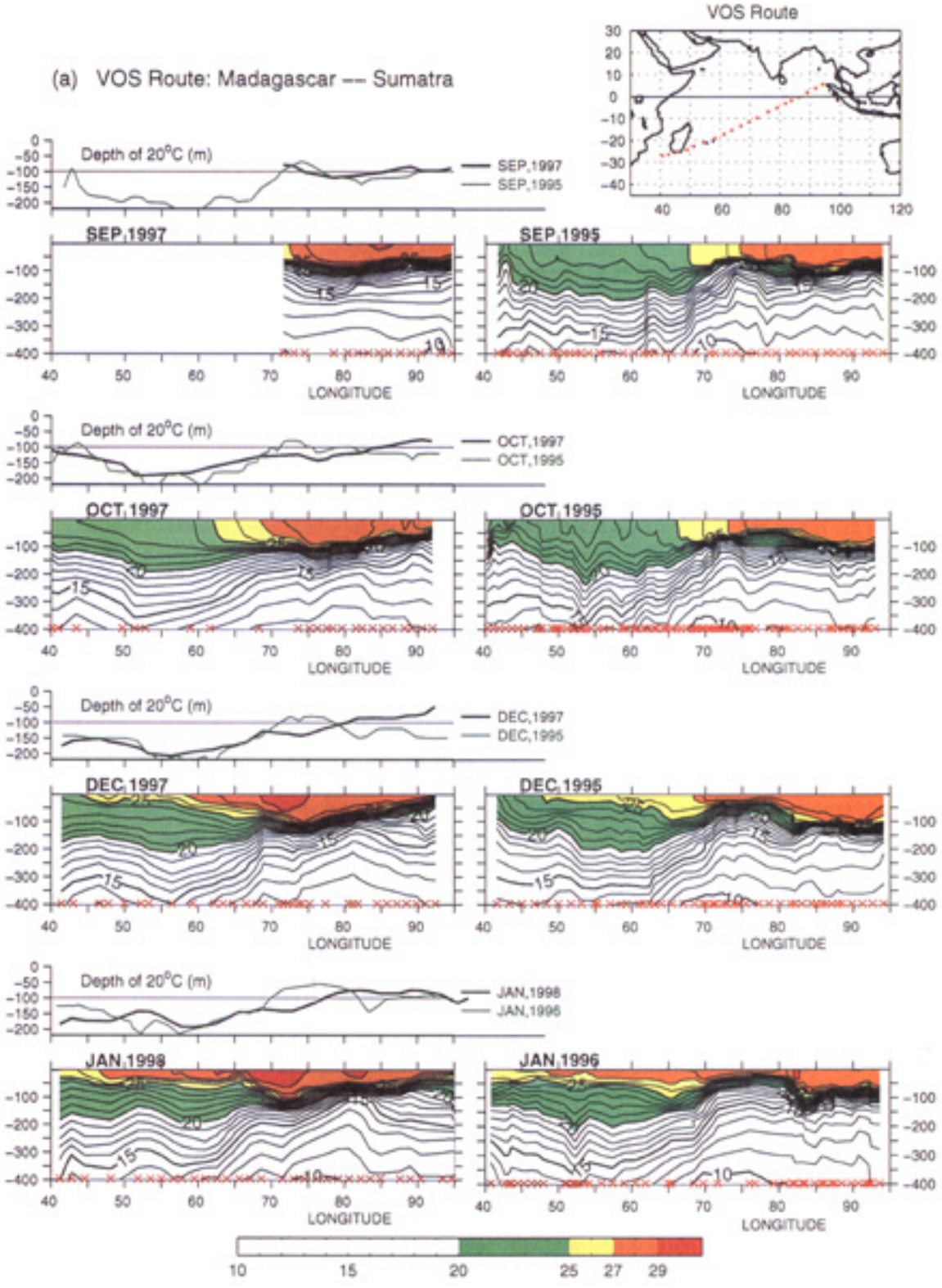

Plate 2. The upper ocean temperature structures in 1997–1998 and 1995–1996 along the VOS routes between (a) Madagascar and Sumatra and (b) Somalia and Australia. The actual VOS routes are plotted at the top right corner. The XBT locations are denoted by red crosses. Temperatures are colored if $> 20°C$. The depths of the 20°C isotherm are also displayed.

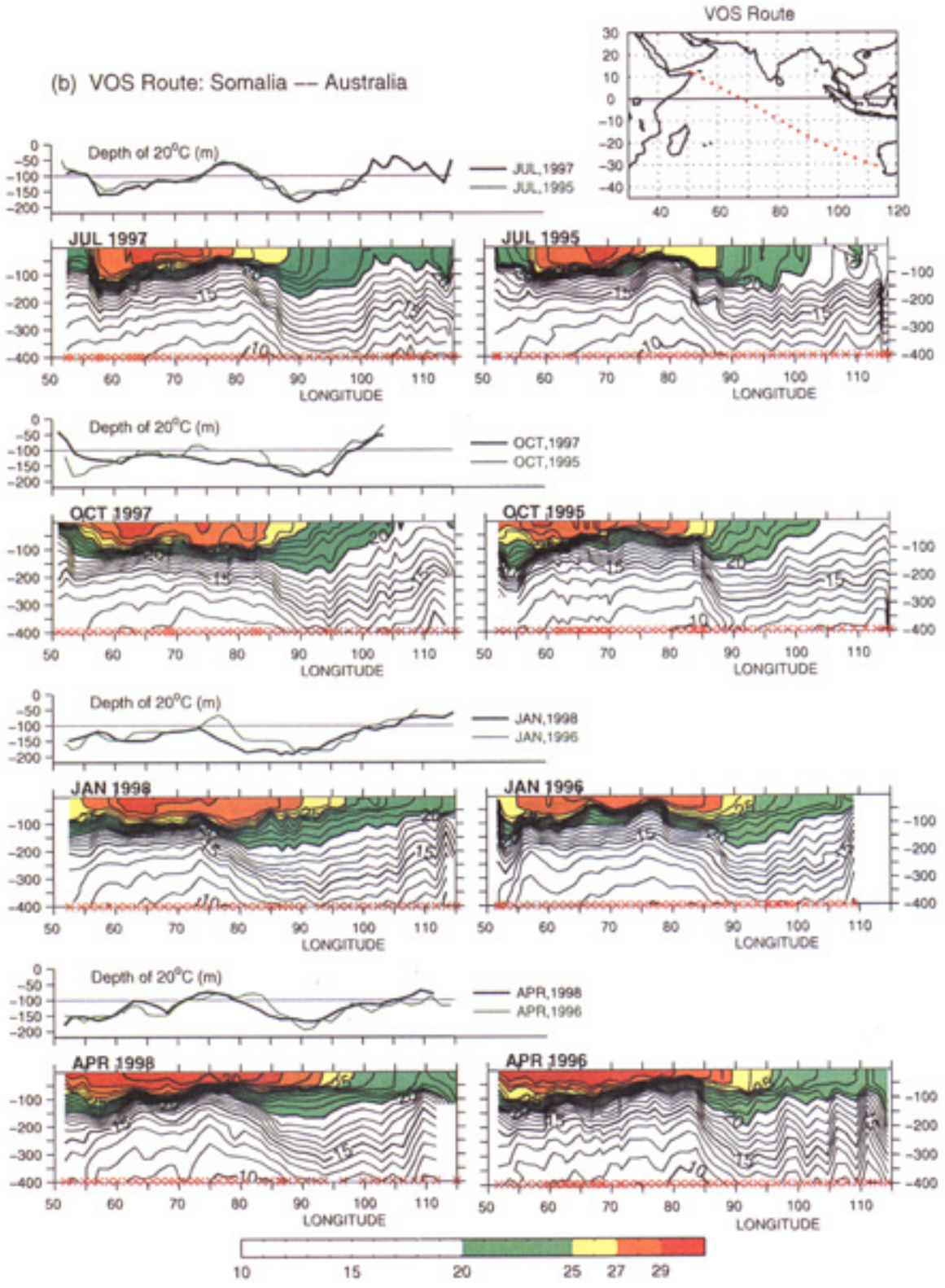

Plate 2. Continued

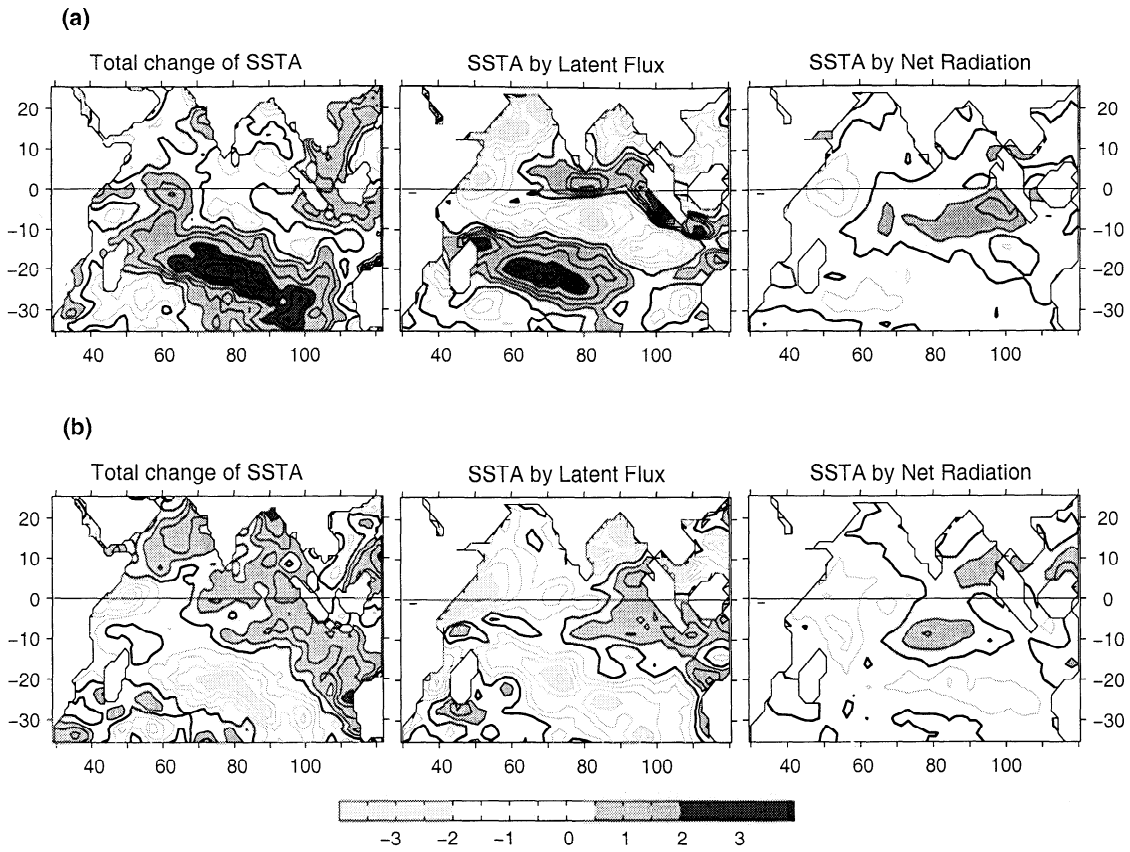

Figure 8. The change of SSTA, latent flux anomalies, and the net radiation flux anomalies integrated over two periods: (a) July–December 1997 and (b) January–May 1998. The anomalies are darkly shaded if $> 0.5°C$ and lightly shaded if $< -0.5°C$. The contour interval is 0.5°C.

Indian Ocean Walker Circulation. However, the cloud structure simulated by an atmospheric general circulation model (AGCM) might contain large uncertainty because of the imperfect paramcterization of moisture processes. Since the amplitude of the radiative flux is small, the noise in the reanalyses places a severe limitation on quantifying the radiative effects. This data set may be combined with satellite-derived outgoing longwave radiation (OLR) to diagnose qualitatively the primary areas affected by the radiative flux. Preliminary investigation of OLR data (not shown) indicates that the radiative flux would have a warming effect on SST in the eastern equatorial region/Bay of Bengal and a cooling effect in the western Indian basin/Arabian Sea. This is consistent with Figure 8, although the degree of the influence remains to be examined.

5.3. Quality of the NCEP Fluxes

The NCEP fluxes are the only flux data available to our present analyses. However, the NCEP products, on monthly average, may contain an error as large as 50 W m^{-2} as a result of underestimated shortwave heating and longwave cooling and overestimated latent cooling and rainfall [*Weller et al.*, 1998]. The resulting error in SST would be at 0.5°C if assuming a mixed layer depth of 60 m. Figure 8 shows that the integrated change of SSTA in the Arabian Sea and Bay of Bengal cannot be explained by either latent or radiation fluxes, as these fluxes had an opposite effect on the regional SST changes. This implies that ocean processes might be a major contributor to the regional SST dynamics and/or the diagnosed NCEP fluxes might be incorrect. The available data are not adequate to quantify the role of oceanic processes, nor are flux observations available to validate the NCEP products during this period. However, as noted above, upwelling processes were crucial in defining the SST off Sumatra during the later half of 1997. Examination of the NCEP wind field points out that the NCEP wind speed anomalies in the Arabian Sea and Bay of Bengal had opposite signs to those calculated from the SSMI and Florida State University (FSU) products, although the structure and intensity of the wind variations in the Southern Ocean agreed remarkably well. Care should be taken in using the NCEP fluxes as the wrong sign of the NCEP wind speed anomalies would inevitably lead to an erroneous latent heat flux.

6. Subsurface Variations Along Two VOS Routes

We utilize the temperature profiles acquired along two cross-basin VOS routes, one between Madagascar and Sumatra (Plate 2a) and the other between Somalia and Shark Bay in Australia (Plate 2b) to illustrate the upper ocean temperature structures in the Indian Ocean. The change of the upper ocean between July 1997 and May 1998 is analyzed and compared with the structure in 1995–1996 of the same months. Data were not available every month. In some months the data were acquired only along a partial route. We present in Plates 2a–2b the sections that enable a direct comparison between 1997–1998 and 1995–1996. The depth of the 20°C isotherm, a commonly used index for the change of the thermocline, is also displayed.

The VOS line between Madagascar and Sumatra (Plate 2a) crossed major SST and SSH anomaly centers in the southern basin and the eastern equatorial region (Figures 4–5). Substantial changes in the temperature structure were observed along this line. The shoaling of the thermocline in the eastern equatorial region was visible in September 1997, as the depth of 20°C isotherm within the longitudes of 80°–90°E was shallower. The change became significant with time. In December 1997 the thermocline east of 80°E was elevated by more than 80 m, while it was depressed by ~50 m between 70° and 80°E. This is consistent with the features shown in the SSH field (Figure 5). The upwelling in the eastern equatorial region lifted the thermocline and lowered the SSH, while the downwelling in the west depressed the thermocline and increased the SSH. In January 1998 the equatorial upwelling was weakened, and so, the thermocline depth was returning to normal. The thermocline was still deep between 70° and 80°E as the strength of the downwelling center south of the equator was largely maintained at that time.

Along this line the large change of the subsurface temperature in association with the shallowing of the thermocline (upwelling) in the eastern basin was clearly seen. There the temperature at 100 m below the surface in December 1997 was ~ 6°–7°C colder than that in December 1995. This is also seen in the equatorial analysis of *Anderson* [1999]. Meanwhile, the surface warming of the southern basin in late 1997 and early 1998 was also visible. For example, the layer in the upper 50 m in January 1998 was ~ 1°C warmer, and the warming was rather uniform. It is worth noting that the region of maximum warming did not match exactly the greatest thermocline anomaly. The thermocline deepening coincided with the downwelling center just south of the equator (WMLL99), while the enhanced warming lay southwestward, in good agreement with the SST anomaly distribution without penetrating to the thermocline (Figure 4).

The VOS line between Somalia and Australia (Plate 2b) lay largely on the edges of major SST and SSH anomaly centers. The changes of the thermocline along this line were not as dramatic as those shown in Plate 2a. Nevertheless, the deepening of the thermocline associated with the downwelling center south of the equator was visible between 70° and 90°E. The locations of the thermocline elsewhere seemed to agree well with those in 1995–1996, indicating that the thermocline in the region did not undergo major changes. Nevertheless, the change of the temperature above the thermocline was substantial, especially since January 1998. The shallow surface layer (within the upper 100 m) was uniformly warmed by > 1°C. The confinement of the warming in the upper layer suggests that the temperature change was largely induced by the incoming surface fluxes and that the mixed layer processes played a major role in the warming. This supports our analysis in section 5 that the warming outside of the equatorial region was a direct response to the change of the latent heat flux due to the weakened wind. The weakened wind would also have weakened the mixing process in the upper ocean and was a positive factor in trapping the heating in the shallow surface layer.

7. Summary and Discussion

The Indian Ocean underwent substantial changes in 1997–1998. The observations show not only the appearance of a dipole mode in the tropical region (WMLL99; SGVY99) but also a persistent basin-scale warming (YR99). We present in this study a data analysis of the basin-scale SST variations during the 1997–1998 event. Multiple data sets are used in the analyses. The data include satellite-derived observations of SST, SSH, and surface wind, in situ temperature measurements from VOS, and surface fluxes diagnosed from the model output of NCEP reanalyses.

The analysis shows that the surface warming first developed in the northern and equatorial regions in the boreal spring of 1997. The warming in the Southern Ocean came one season later, in the early summer of 1997. The eastern equatorial region was the only area where abnormal cooling developed during July–December 1997. The negative SST anomalies together with the positive SST anomalies in the western equatorial region formed the dipole mode (e.g., WMLL99; SGVY99). After the regional cooling recessed, warming appeared over the entire Indian Ocean in January 1998 and persisted for more than 6 months. The Indian SST anomalies peaked at two periods: November–December–January and the following April–May–June. The first period coincided with the mature phase of the El Niño in the Pacific. However, the timing of the anomaly peaks had a phase shift with regard to the Niño3 SST anomaly index and is found to be regulated by the Indian Ocean seasonal cycle. SGVY99 and WMLL99 noted the phase locking of the Indian dipole mode to the seasonal cycle. Our analysis shows that outside of the equatorial region, the anomaly peaks were also in phase with the seasonal extrema.

The change of SST in the equatorial ocean was governed by a coupled interaction between the atmosphere and ocean, a mechanism which is postulated as a key to the oscillation of the Indian dipole mode (WMLL99; SGVY99). At the height of the dipole mode the Walker Circulation in the Indian Ocean was reversed. This was manifested as the reversal of the climatological SST along the equator and the appearance of prolonged easterly winds in the equatorial region. The oceanic upwelling and downwelling processes associated with Kelvin waves (for the former) and Rossby waves (for the latter) contributed to the surface cooling in the east and warming in the west. The subsurface temperature structures, constructed from expendable bathythermograph (XBT) profiles acquired along two cross-basin VOS routes, show that the upwelling off the coast of Sumatra elevated the regional thermocline by more than 80 m and allowed sufficient cold water to upwell to the upper layer. This affected not only SST but also subsurface temperatures. The temperature at 100 m in December 1997 was ~6–7°C colder than that in December 1995.

The change of SST in the southern Indian Ocean was largely a direct response to the change of local air–sea fluxes, particularly the latent flux component. During boreal fall–winter of 1997 the southeasterly trades were displaced abnormally prolonged in their northmost equatorial position in association with the reversed Walker Circulation. This shifted the center (and so the maximum intensity) of the trades more toward the equator and weakened the winds in the central Southern Ocean. The weakened winds resulted in a major reduction in the latent heat release and provided the source for the surface warming. Meanwhile, the weakened winds would also have weakened the mixing in the upper ocean and trapped the warming in the shallow upper layer. The cross-basin upper ocean temperature sections show that the extratropical warming in 1997–1998 was rather uniformly distributed in the upper 60 m, indicating the role of mixed layer processes in the warming. By setting the mixed layer depth to be 60 m the total change of the SST anomalies integrated over the two periods, i.e., July–December 1997 and January–May 1998 were explained well by the intensity and pattern of the latent flux anomalies integrated over the same two periods.

The NCEP fluxes are the only flux data available for the present analysis. We found that the NCEP latent flux can explain well the change of the SST in the southern Indian Ocean but fails in the Arabian Sea and the Bay of Bengal. Since the change of latent flux is largely determined by the change of wind speed in the tropical regions [*Liu and Gautier*, 1990, *Lau et al.*, 1997], we have conducted comparisons of the NCEP surface wind product with the SSMI wind product and the wind derived from the FSU pseudostress for the period of 1997–1998. The comparisons show that the NCEP wind speed anomalies were in good agreement with SSMI and FSU winds in the southern basin but had the wrong sign over large area of the northern basin. The questionable wind in the northern basin could certainly introduce a considerable degree of uncertainty in the diagnosed fluxes. In addition, solar and longwave radiations need to be calibrated before their effects on the basin-scale warming can be quantified. The fluxes from the NCEP and other reanalyses centers could be a valuable source for climate studies after being calibrated and validated against high-quality in situ flux observations.

Acknowledgments. This study was supported by NASA's Global Modeling and Analysis Program for the NASA Seasonal-to-Interannual Prediction Project (NSIPP). L. Yu also thanks the support from the NASA QuikScat Program under grant 1207962 from the Jet Propulsion Laboratory, California Institute of Technology. Dick Reynolds is thanked for providing the SST analyses, David Adamec and Ken Casey for the gridded TOPEX/Poseidon SSH, and Bob Atlas and Joe Ardizone for the gridded SSMI wind products. The NCEP diagnosed air-sea heat fluxes are downloaded from the NCEP ftp site: ftp.cdc.noaa.gov/cdc/reanalysis. Peter Webster and an anonymous reviewer are sincerely thanked for their constructive and thoughtful comments, which led to an improved presentation of the manuscript. We benefited from discussions with Eugene Rasmusson, Tim Liu, Bob Weller, Steve Anderson, and Bill Lau. WHOI contribution number 10135.

References

Adamec, D., Modulation of the seasonal signal of the Kuroshio extension during 1994 from satellite data, *J. Geophys. Res., 103*, 10,209–10,222, 1998.

Anderson, D., Extremes in the Indian Ocean, *Nature, 401*, 337–338, 1999.

Atlas, R., R. N. Hoffman, and S. C. Bloom, Surface wind velocities over the ocean, in *Atlas of Satellite Observations Related to Global Change*, edited by R. J. Gurney, J. L. Foster, and C. L. Parkinson, pp. 128–139, Cambridge Univ. Press, New York, 1993.

Bjerknes, J., Atmospheric teleconnections from the equatorial Pacific, *Mon. Weather Rev., 97*, 163–172, 1969.

Cadet, D. L., The Southern Oscillation over the Indian Ocean, *J. Clim., 5*, 189–212, 1985.

Cane, M. A., On the dynamics of equatorial currents with application to the Indian Ocean, *Deep Sea Res., Part A, 27*, 525–544, 1980.

Chambers, D. P., B. D. Tapley, and R. H. Stewart, Anomalous warming in the Indian Ocean coincident with El Niño, *J. Geophys. Res., 104*, 3035–3047, 1999.

Gautier, C., P. Peterson, and C. Jones, Variability of air–sea interactions over the Indian Ocean derived from satellite observations, *J. Clim., 11*, 1859–1873, 1998.

Kalnay, E., et al., The NCEP/NCAR reanalysis project, *Bull. Am. Meteorol. Soc., 77*, 437–471, 1996.

Kapala, A., K. Born, and H. Flohn, Monsoon anomaly or an El Niño in the equatorial Indian Ocean? Catastrophic rains in East Africa and their teleconnections, papers presented at International Conference on Monsoon Variability and Prediction, World Meteorol. Org., Trieste, Italy, May 3–13, 1994.

Latif, M., D. Dommenget, M. Dima, and A. Grotzner, The role of Indian Ocean sea surface temperature in forcing East African rainfall anomalies during December–January 1997/98, *J. Clim., 12*, 3497–3504, 1999.

Lau, K.-M., and H.-T. Wu, An assessment of the impact of

the 1997–98 El Nino on the Asian-Australian Monsoon, *Geophys. Res. Lett., 26*, 1747–1750, 1999.

Lau, K.-M., H.-T. Wu, and S. Bony, The role of large-scale atmospheric circulation in the relationship between tropical convection and sea surface temperature, *J. Clim., 10*, 381–392, 1997.

Liu, W. T., and C. Gautier, Thermal forcing on the tropical Pacific from satellite data, *J. Geophys. Res., 95*, 13,209–13,217, 1990.

Liu, T. W., A. Zhang, and J. K. B. Bishop, Evaporation and solar irradiance as regulators of sea surface temperature in annual and interannual changes, *J. Geophys. Res., 99*, 12,623–12,637, 1994.

McCreary, J. P., P. K. Kundu, and R. L. Molinari, A numerical investigation of dynamics, thermodynamics and mixed-layer processes in the Indian Ocean, *Prog. Oceanogr., 31*, 181–244, 1993.

McPhaden, M. J., The child prodigy of 1997–98, *Nature, 398*, 559–562, 1999.

Murtugudde, R., J. McCreary, and A. Busalacchi, Oceanic processes associated with anomalous events in the Indian Ocean with relevance to 1997–1998, *J. Geophys. Res., 105*, 3295–3306, 2000.

Nicholls, N., Air–sea interaction and the quasi-biennial oscillation, *Mon. Weather Rev., 106*, 1505–1508, 1978.

Nicholls, N., All-India summer monsoon rainfall and sea surface temperature around northern Australia and Indonesia, *J. Clim., 8*, 1463–1467, 1995.

Nicholson, S. E., An analysis of the ENSO signal in the tropical Atlantic and western Indian Oceans, *Int. J. Climatol., 17*, 345–375, 1997.

Nigam, S., and H. S. Shen, Structure of atmospheric low-frequency variability over the tropical Pacific and Indian Oceans, part I, COADS observations, *J. Clim., 6*, 657–676, 1993.

Philander, S. G. H., *El Niño, La Niña, and the Southern Oscillation*, 293 pp., Academic, San Diego, Calif., 1990.

Rasmusson, E. M., and T. H. Carpenter, Variations in tropical sea surface and surface wind fields associated with the Southern Oscillation/El Niño, *Mon. Weather Rev., 110*, 354–384, 1982.

Rasmusson, E. M., and J. M. Wallace, Meteorological aspects of the El Niño/Southern Oscillation, *Science, 222*, 1195–1202, 1983.

Reverdin, G., D. Cadet, and D. Gutzler, Interannual displacements of convection and surface circulation over the equatorial Indian Ocean, *Q. J. R. Meteorol. Soc., 122*, 43–67, 1986.

Reynolds, R. W., and T. M. Smith, A high resolution global sea surface temperature climatology, *J. Clim., 8*, 1572–1583, 1995.

Saji, N. N., B. N. Goswami, P. N. Vinayachandran, and T. Yamagata, A dipole mode in the tropical Indian Ocean, *Nature, 401*, 360–363, 1999.

Shukla, J., Interannual variability of monsoons, in *Monsoon*, edited by J. S. Fein and P. L. Stephens, pp. 399–464, John Wiley New York, 1987.

Tourre, Y. M., and W. B. White, ENSO signals in global upper-ocean temperature, *J. Phys. Oceanogr., 25*, 1317–1332, 1995.

Tourre, Y. M., and W. B. White, Evolution of ENSO signals over the Indo-Pacific domain, *J. Phys. Oceanogr., 27*, 683–696, 1997.

Webster, P. J., The variable and interactive monsoon, in *Monsoon*, edited by J. S. Fein and P. L. Stephens, pp. 269–330, John Wiley New York, 1987.

Webster, P. J., and R. Lukas, TOGA-COARE: the Coupled Ocean–Atmosphere response experiment, *Bull. Am. Meteorol. Soc., 73*, 1377–1416, 1992.

Webster, P. J., A. Moore, J. Loschnigg, and R. Leben, Coupled ocean-atmosphere dynamics in the Indian Ocean during 1997–1998, *Nature, 401*, 356–360, 1999.

Weller, R. A., M. F. Baumgartner, S. A. Josey, A. S. Fischer, and J. Kindle, Atmospheric forcing in the Arabian Sea during 1994–95: Observations and comparisons with climatology and models, *Deep Sea Res., 45*, 1961–1999, 1998.

Yang, J., L. Yu, C. Koblinsky, and D. Adamec, Dynamics of the seasonal variations in the Indian Ocean from TOPEX/Poseidon sea surface height and an ocean model, *Geophys. Res. Lett., 25*, 1915–1918, 1998.

Yasunari, T., Global structure of the El Niño/Southern Oscillation, part I, El Niño composites, *J. Meteorol. Soc. Jpn., 65*, 67–80, 1987a.

Yasunari, T., Global structure of the El Niño/Southern Oscillation, part II. Time evolution, *J. Meteorol. Soc. Jpn., 65*, 81–102, 1987b.

Yu, L., and M. Rienecker, Evidence of an extratropical atmospheric influence during the onset of the 1997–98 El Niño, *Geophys. Res. Lett., 25*, 3537–3540, 1998.

Yu, L., and M. Rienecker, Mechanisms for the Indian Ocean warming during the 1997–98 El Niño, *Geophys. Res. Lett., 26*, 735–738, 1999.

L. Yu, Department of Physical Oceanography, Woods Hole Oceanographic Institution, Woods Hole, MA 02543. (lyu@whoi.edu)

M. M. Rienecker, Oceans and Ice Branch, Laboratory of Hydrospheric Processes, NASA Goddard Space Flight Center, Greenbelt, MD 20771. (rienecke@gsfc.nasa.gov)

(Received June 28, 1999; revised January 31, 2000; accepted March 24, 2000.)